Direct measurement of the transition from edge to core power coupling in a light-ion helicon source

P. A. Piotrowicz, J. F. Caneses, M. A. Showers, D. L. Green, R. H. Goulding, J. B. O. Caughman, T. M. Biewer, J. Rapp, and D. N. Ruzic

Citation: Physics of Plasmas **25**, 052101 (2018); doi: 10.1063/1.5023924
View online: https://doi.org/10.1063/1.5023924
View Table of Contents: http://aip.scitation.org/toc/php/25/5
Published by the American Institute of Physics

PHYSICS OF PLASMAS 25, 052101 (2018)

Direct measurement of the transition from edge to core power coupling in a light-ion helicon source

P. A. Piotrowicz,[1,a)] J. F. Caneses,[2,b)] M. A. Showers,[2] D. L. Green,[3] R. H. Goulding,[3] J. B. O. Caughman,[3] T. M. Biewer,[3] J. Rapp,[3] and D. N. Ruzic[1]
[1]*University of Illinois in Urbana-Champaign, Champaign, Illinois 61801, USA*
[2]*University of Tennessee, Knoxville, Tennessee 37996, USA*
[3]*Oak Ridge National Laboratory, Oak Ridge, Tennessee 37831, USA*

(Received 29 January 2018; accepted 16 April 2018; published online 2 May 2018)

We present time-resolved measurements of an edge-to-core power transition in a light-ion (deuterium) helicon discharge in the form of infra-red camera imaging of a thin stainless steel target plate on the Proto-Material Exposure eXperiment device. The time-resolved images measure the two-dimensional distribution of power deposition in the helicon discharge. The discharge displays a mode transition characterized by a significant increase in the on-axis electron density and core power coupling, suppression of edge power coupling, and the formation of a fast-wave radial eigenmode. Although the self-consistent mechanism that drives this transition is not yet understood, the edge-to-core power transition displays characteristics that are consistent with the discharge entering a slow-wave anti-resonant regime. RF magnetic field measurements made across the plasma column, together with the power deposition results, provide direct evidence to support the suppression of the slow-wave in favor of core plasma production by the fast-wave in a light-ion helicon source. *Published by AIP Publishing*. https://doi.org/10.1063/1.5023924

I. INTRODUCTION

Helicon sources are known to be effective at producing high-density plasmas and have found practical applications in the areas of semiconductor processing,[1,2] space propulsion,[3,4] fusion-relevant plasma material interaction (PMI) research,[5,6] and negative ion source development for neutral beam injectors (NBIs).[7,8] Recently, the PMI, NBI, and space propulsion communities have taken special interest in using helicon sources to create high-density light-ion plasmas. In this letter, we present experimental observations of an edge-to-core power coupling transition in a high electron density ($n_e \approx 4 \times 10^{19}\,\mathrm{m}^{-3}$), light-ion helicon source. We present evidence that the helicon mode, bounded fast-wave, reproducibly deposits significant power in the plasma core which delivers heat fluxes up to $0.6\,\mathrm{MW\ m}^{-2}$ to a plasma-facing target. An interpretation of the result is provided using the existing theory.[9]

Attempts to identify the physical mechanisms of the high ionization efficiency of the helicon source have been a point of interest in the literature.[10–15] Most authors agree that the efficient ionization of helicon sources using heavy ions is due to mode conversion of fast-waves into the Trivelpiece-Gould mode (TG), bounded slow-wave (SW), at the plasma edge;[9,12,16–18] therefore, power deposition is typically edge dominated in helicon sources using heavy ions. However, regardless of where the power coupling occurs, heavy-ion discharges typically have centrally peaked electron density profiles. This apparent paradox can be explained by the short circuit effect[17,19] mediated by unmagnetized ions.

There are two main aspects that make light-ion helicon sources different from heavy-ion sources: ion magnetization and the effect of the lower hybrid resonance (LHR). At high densities, the lower hybrid resonance has the effect of restricting the slow-wave to a very thin layer in the plasma periphery and creates an evanescent layer between the fast-wave in the high plasma density region (core) and the slow-wave in the low plasma density region (edge) of the discharge.[20] Ion magnetization precludes transport effects that cause centrally peaked electron density profiles in heavy-ion discharges.[17,19] Therefore, in discharges with strongly magnetized ions and electrons, production of centrally peaked density profiles necessitates the deposition of power directly in the core. This mechanism is only accessible via the fast-wave.

In what follows, results are presented from the light-ion helicon source in the Prototype Material Exposure eXperiment (Proto-MPEX).[6] An improved mode of operation has been recently observed[6,21] and is characterized by a significant increase in the on-axis electron density ($n_e \approx 1$–$4 \times 10^{19}\,\mathrm{m}^{-3}$), a change in the radial density profile from hollow to centrally peaked, and a change in the radial electron temperature profile from hollow to flat. Evidence is presented here to show that the improved mode of operation is due to strong power coupling to the core plasma via the fast-wave and suppression of mode conversion to the slow-wave at the edge. Radial eigenmode formation of the fast-wave is concurrently observed with the transition from edge to core power coupling in the plasma column. Section II will go over a description of the experiment and the infra-red (IR) imaging system used. In Sec. III, the observations made by the IR camera of the edge to core power transition will be presented along with B-dot probe measurements. Section IV will cover a theoretical explanation of these observations. Concluding remarks are made in Sec. V.

[a)]Electronic mail: ppiotr3@illinois.edu
[b)]Electronic mail: canesesmarjf@ornl.gov

II. EXPERIMENT

A schematic of the Proto-MPEX device is shown in Fig. 1. Details of the setup are provided in Ref. 6. For the experiments reported herein, the DC magnetic fields at the helicon source and target location are approximately 0.05 T and 0.6 T, respectively. The driving frequency of the helicon antenna is 13.56 MHz and is powered with 110 kW for a 300 ms pulse length. The helicon antenna is a 25 cm long, right-handed helical fractional turn design. Deuterium gas is injected behind the helicon antenna at a rate of 2.32 standard liters per minute (SLM) 300 ms before the RF pulse and reduced to 0.8 SLM 50 ms before the RF pulse. Double Langmuir probes[22] that are scanned radially are used to measure the electron density at axial locations A and B. At these same axial locations, RF magnetic field profiles are measured using B-dot probes.[23,24] A thin (0.01 in.) stainless steel (SS) plasma-facing target plate is located at the end of the device at z = 4.3 m.

Two-dimensional (2D) infra-red imaging of the target plate is performed using a FLIR A655sc IR camera, whose parameters are detailed in Ref. 25. The frame rate of the IR camera is 50 Hz (0.02 s). The timescale on which this measurement is taken, as well as the heat diffusion constant of the SS target, allows ignoring radial and azimuthal heat diffusion within the target plate by satisfying $\frac{\partial T}{\partial t} \gg D(\nabla_\perp^2 T)$ Therefore, the time-differentiated thermal images give a two-dimensional (2D) profile of the plasma heat flux as determined by the following equation:

$$\frac{\partial T}{\partial t} = \frac{q_v}{\rho c_p}, \tag{1}$$

where T is the temperature measured by the IR camera, c_p and ρ are the specific heat and density of SS, t is the time, and q_v is the volumetric heat source which, in the case of a plasma heat flux on the surface, is written as $q_v(r,\phi,z) = q_s(r,\phi)\delta(z-z_0)$, where z_0 is the location of the target.

In the presence of strong magnetic fields, it can be shown that radial electron heat transport can be neglected in comparison to axial heat transport. For typical Proto-MPEX plasma conditions, it can be shown that for electrons, $q_\parallel/q_\perp \gg L/R$, where $q_\parallel/q_\perp = (\omega_{ce}/\nu_e)^2 \frac{\nabla_\parallel T_e}{\nabla_\perp T_e}$ is the ratio of parallel to perpendicular electron heat flux.[26] The electron cyclotron frequency is ω_{ce}, ν_e is the electron collision frequency, T_e is the electron temperature, L is the length from the antenna to the target, and $R \approx 1$ mm is the characteristic radial scale of the measurement. Since the condition given above is satisfied, the plasma heat flux inferred from the IR emission profile on the target plate can be mapped back to the deposited heat upstream along the magnetic flux lines. This mapping is a good approximation of the origin of the power deposition.

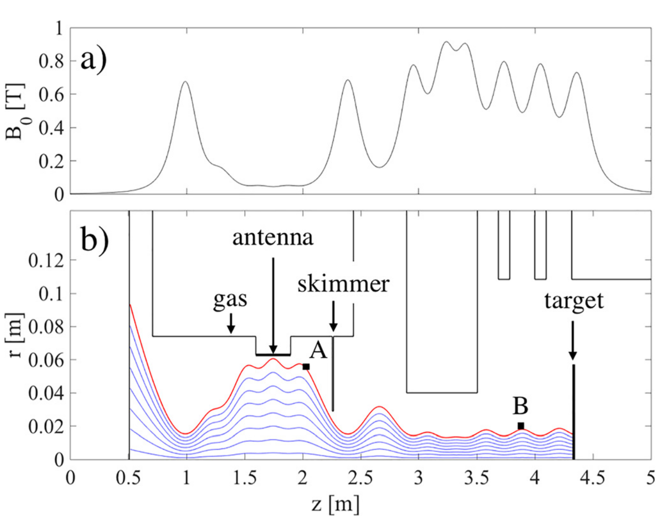

FIG. 1. (a) On axis magnetic field strength in Proto-MPEX for the magnetic configuration used. (b) Flux line mapping and a two dimensional schematic of Proto-MPEX.

III. OBSERVATIONS

The heat flux to the target plate is shown in Fig. 2. The two-dimensional distributions of the heat fluxes at the start and end of the RF pulse are shown in panels (a) and (b), respectively. At the start (end) of the RF pulse, the heat flux is dominated by power deposition at the edge (core) of the plasma column. As is evident in panel (d), a transition is observed at approximately $t = 4.25$ s, where the edge power deposition is suppressed and the core deposition begins to dominate. At the end of the pulse, the core power deposition is clearly dominant and delivers up to 0.6 MW m^{-2} to the target plate. Extensive experimentation using a helicon power of 100 kW has shown that this edge-to-core transition can be reliably produced on demand provided that (a) the neutral gas is puffed at the location of the antenna about 300 ms before

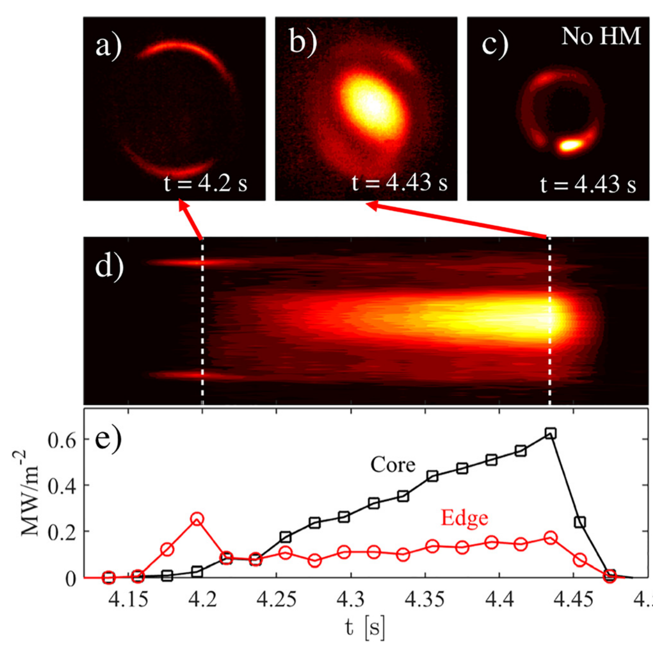

FIG. 2. Heat flux to the target inferred from IR thermography (a) at the start of the RF pulse (t = 4.2 s) and (b) at the end of the RF pulse (t = 4.43 s). The length scale of the y and x axes is 4 cm across the image. Parts (a), (b), and (d) are the same discharge. Part (c) shows the end of the RF pulse (t = 4.43 s) in a condition where the discharge did not transition to core power deposition. Part (d) shows the time evolution of the heat flux to the target. Part (e) shows the time evolution of the heat flux to the target at the core (center of the image) and at the edge (location of the largest heat flux at t = 4.2 s).

the RF pulse, (b) the neutral pressure before breakdown is 2–3 Pa, and (c) the discharge is at least 100 ms in duration.

At the time of the increased core power coupling, measurements performed near the helicon antenna (location A) with RF magnetic (B-dot) probes indicate (1) an increase in fast-wave energy density in the core plasma and (2) the formation of a fast-wave radial eigenmode. Presented in Fig. 3(a) is the magnitude of the B_r wave field component on axis and at the edge of the discharge. Conditions are identical to those associated with Fig. 2. At the same time, as the transition from edge-to-core power deposition as seen in Fig. 2, the on-axis RF magnetic energy $|B_r|^2$ increases, while the edge magnetic energy decreases. Figure 3(b) shows the on-axis electron density and temperature measurements at locations A and B of Fig. 1. From this, we can see that once the core heating is established, there is a correspondingly high plasma density at the source and the target location.

Figure 4 presents a radial scan of the B_z component of the fast-wave measured near the helicon antenna (location A) during a core-heated discharge. Experimental conditions are similar to those associated with Fig. 2. The measurements in Fig. 4 indicate the presence of a radial eigenmode: (a) the radial variation of the magnitude displays the characteristic bimodal shape of the B_z (m = +1) component of the helicon mode and (b) the radial phase variation has the characteristic 180° phase shift on-axis. It is worth noting that before the edge-to-core transition or when this transition does not occur, both the amplitude and phase of the RF wave fields strongly fluctuate, and no clear indication of a radial eigenmode is observed.

IV. DISCUSSION

The experimental observations described in Sec. III show that a transition of power coupling from the edge to the core is simultaneously accompanied by the formation of a fast-wave radial eigenmode. In this section, these observations

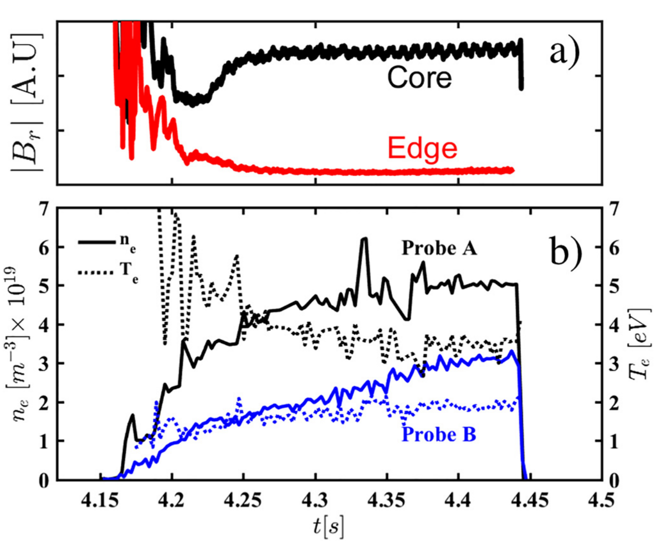

FIG. 3. (a) B_r component of the fast-wave measured near the helicon antenna (location A) on-axis (black) and at the edge (red) of the plasma column. (b) On-axis electron density (solid line) and temperature (dotted line) measured at location A (black) and location B (blue).

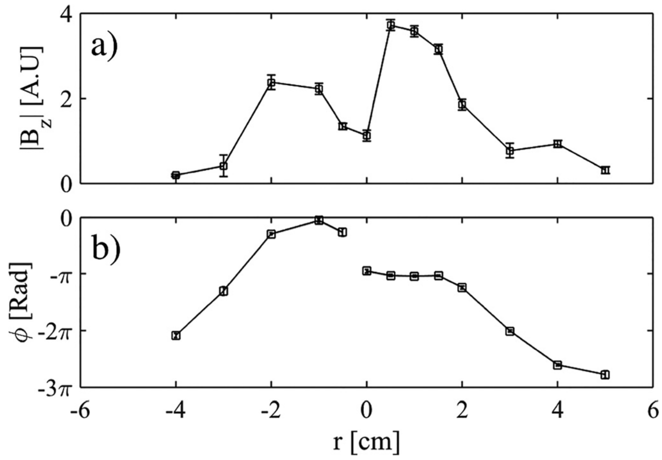

FIG. 4. Radial variation of B_z measured with a RF (B-dot) probe at location A at the end of a 150 ms RF pulse: (a) magnitude and (b) phase. The DC magnetic fields at the source and target are 0.05 T and 0.6 T, respectively, and D_2 gas is injected at location A.

will be related to the theoretical predictions made in Ref. 9, which predict anti-resonance regimes of the fast and slow-waves in the analytic treatment of a homogeneous plasma column bounded by a dielectric gap and an outer conductor. In this condition, the RF fields of the wave in anti-resonance are reduced, and less power is absorbed by the plasma from that wave. Therefore, a slow-wave anti-resonance results in a reduction in edge power deposition which allows for more energy available to the fast-wave, which would cause increased core power deposition. In a more complicated picture of a plasma column with a density gradient, the slow-wave anti-resonance can be understood as a reduction of non-resonant mode conversion to the slow-wave by the reduction of the fast-wave amplitude at the edge of the plasma column, and this process is explained in Ref. 18. The analytic form of a slow-wave anti-resonance satisfies the bounded dispersion condition given by Eq. (2),

$$J'_m(k_\perp R_p) + \frac{m}{k_z R_p} J_m(k_\perp R_p) = 0, \tag{2}$$

$$k_\perp = \frac{\omega_{pe}^2}{\omega\omega_{ce}} \frac{k_0^2}{k_z}. \tag{3}$$

The plasma frequency is ω_{pe}, k_0 is the vacuum wavenumber, m is the azimuthal mode, k_z is the axial wavenumber of the eigenmode, J_m is the mth order Bessel function, and $J_m(x)'$ is the derivative of $J_m(x)$.

Figure 5 displays (a) the cold plasma dispersion relation relevant to our experimental conditions as a function of electron density and (b) a typical radial electron density profile associated with Fig. 5 measured at the helicon source (location A). Since the lower hybrid resonance (LHR) restricts the propagation of the slow-wave to the edge region where the electron density is less than $10^{16}\ \mathrm{m}^{-3}$, any power deposition and/or RF wave fields in the plasma core must be attributed to the fast-wave. Since the discharge equilibrium after the transition satisfies Eq. (2) for the RF B_z component and the dispersion relation only allows the propagation of the fast wave inside the core plasma, we believe that the plasma

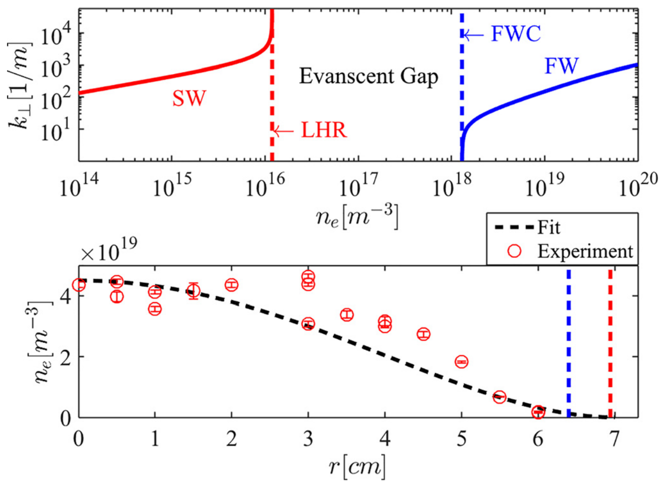

FIG. 5. (Top) Transverse wavelength of the slow-wave (SW) and the fast-wave (FW) calculated from the cold plasma dispersion relation assuming $k_z = 20\,\mathrm{m}^{-1}$, $B_0 = 0.05$ T, and atomic deuterium ions. (Bottom) Electron density radial profile measured at location A from Fig. 1. The radial locations of the lower hybrid resonance (LHR) and the fast-wave cutoff (FWC) are shown assuming a density profile fit of $n_e(r) = n_e^{max}(1-(r/R_p)^2)^2 + n_e^{edge}$, where $n_e^{max} = 4.5\times10^{19}\,\mathrm{m}^{-3}$, $n_e^{edge} = 1\times10^{16}\,\mathrm{m}^{-3}$, and $R_p = 7\,\mathrm{cm}$.

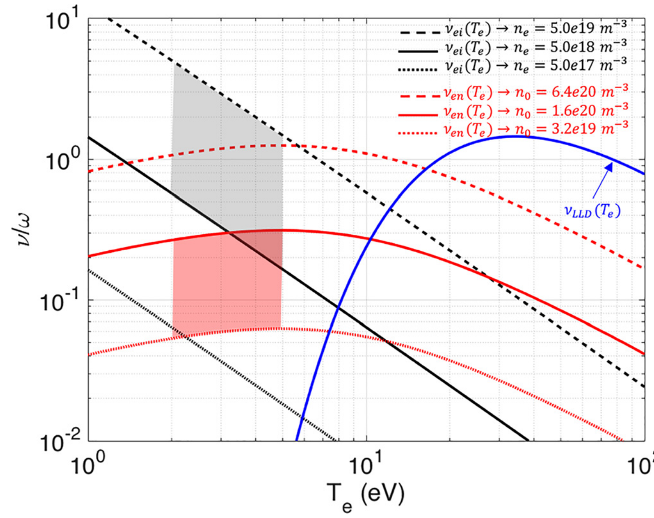

FIG. 6. Normalized collision frequency as a function of electron temperature (T_e) for electron-ion Coulomb (black) and electron-neutral (red) collisions. The effective collision frequency for linear electron Landau damping is given by the blue curve. The highlighted regions show the relevant regions for Proto-MPEX conditions.

production is fast-wave dominated and call this a "helicon-mode" discharge.

The self-consistent mechanism that drives the edge-to-core transition is still an open question. However, previous simulation[27] of a light-ion helicon source with a 2D EM solver and a single fluid plasma transport model shed light on edge-to-core transitions: Edge coupled power at the start of the discharge leads to a hollow plasma density profile. The plasma created at the edge is rapidly lost along magnetic field lines with a short connection length to the wall. However, the edge-produced plasma can diffuse radially inwards and fill in the central region of the plasma column. Eventually, the central density increases to the level at which the fast-wave can propagate in the core. At this point, power is collisionally coupled directly in the plasma core, the plasma is better confined, and the radial density profile becomes centrally peaked. However, this simulation lacked a self-consistent calculation of neutral density and electron temperature to comment on the role of the neutrals. The neutral gas dynamics plays an important role in the transition to the "helicon mode" in Proto-MPEX, since this mode of operation is only observed when a specific gas puffing recipe is utilized.[6,21]

From a purely electromagnetic point of view, an important observation from the IR measurements in Fig. 2 is the suppression in edge power deposition in favour of core deposition. This suppression effect is predicted theoretically in Ref. 18 when discharge conditions allow the formation of eigenmodes of the fast-wave. We can also conclude from these observations that the efficient plasma production in the Proto-MPEX "helicon-mode" is fast wave dominated.

The damping mechanism of the fast-wave in helicon sources has been a point of discussion in the literature.[11,13,15] Collisional damping and isotropic heating of electrons by the fast-wave are typically not considered efficient mechanisms to heat electrons. However, with the high electron density and relatively low electron temperature produced in Proto-MPEX, it is a good candidate to be the dominant mechanism of power coupling to the electrons. Figure 6 shows the normalized collision frequencies calculated, for electron-ion Coulomb and electron D_2 neutral collisions, as a function of electron temperature. The effective collision frequency for linear electron Landau damping[28] is also shown in this figure. From this figure, we see that for the conditions present in Proto-MPEX ($n_e \approx 5\times10^{19}\,\mathrm{m}^{-3}$, $T_e < 10$ eV), Coulomb collisions are the dominant linear damping mechanism for coupling power from the fast-wave to the electrons. Several authors were able to explain the damping of the fast-wave in high density light-ion plasmas with a calculated collisional damping given by electron neutral and Coulomb collisions.[5,27,29]

However, the authors admit that since diagnostic access limits accessing the region directly under the helicon antenna, measurements of the gradients of electron density and temperature in this region are absent. This leaves the possibility of electron temperature increasing to values where collisional damping is no longer an effective damping mechanism of the fast-wave. Non-linear heating mechanisms, such as the parametric decay of the fast-wave into electron plasma and ion-sound waves,[15,30] have also been proposed to heat the electrons in helicon sources. Reference 30 estimated that the damping of the fast-wave due to excitation of ion-sound turbulence and subsequent turbulent electron heating is more effective at transferring fast-wave power to the electrons than Coulomb collisions for the experimental conditions reported in Ref. 31. Such mechanisms have not yet been explored in light-ion helicon sources. The ion mass dependence of these parametric instabilities seems to increase its effective collision frequency, and so, they might be an important damping mechanism for light-ion helicon sources.

V. CONCLUSION

In summary, an improved "helicon-mode" of operation in Proto-MPEX has been described which is characterized by

(1) an increase in the on-axis electron density up to $4 \times 10^{19}\,\mathrm{m}^{-3}$ at the source location, (2) significant core power coupling, (3) suppression of edge power coupling, and (4) an increase in the fast-wave energy density in the core plasma due to the formation of a fast-wave radial eigenmode. The self-consistent mechanism that drives the edge-to-core transition in ProtoMPEX is not yet understood; however, the transition displays characteristics that are consistent with the plasma column entering a "slow-wave anti-resonance" regime as predicted by Shamrai and Taronov.[9] Evidence to support this hypothesis are based on the IR thermography data and RF magnetic (B-dot) probe data. The IR thermography shows that the increase in core power deposition follows the suppression of the edge contribution. The B-dot probe data show that concurrent with this power transition is an increase in the on-axis magnetic energy and the formation of a radial eigenmode. These results show that in light-ion helicon sources, significant power can be coupled to the core via the fast-wave. Moreover, it is shown that helicon sources have the potential to be used as plasma sources for applications requiring high electron density ($n_e > 4 \times 10^{19}\,\mathrm{m}^{-3}$) in light gases.

ACKNOWLEDGMENTS

This material is based on the work supported by the U.S. Department of Energy, Office of Science, Office of Fusion Energy Sciences, under Contract No. DEAC05-00OR22725.

This manuscript was authored by UT-Battelle, LLC, under Contract No. DE-AC05-00OR22725 with the U.S. Department of Energy. The U.S. Government retains and the publisher, by accepting the article for publication, acknowledges that the U.S. Government retains a non-exclusive, paid-up, irrevocable, world-wide license to publish or reproduce the published form of this manuscript, or allow others to do so, for U.S. Government purposes. The Department of Energy will provide public access to these results of federally sponsored research in accordance with the DOE Public Access Plan (http://energy.gov/downloads/doe-public-access-plan).

[1] F. F. Chen and D. Arnush, "Generalized theory of helicon waves. I. Normal modes," Phys. Plasmas **4**, 3411–3421 (1997).
[2] D. B. Hayden, D. R. Juliano, M. N. Neumann, M. C. Allain, and D. N. Ruzic, "Helicon plasma source for ionized physical vapor deposition," Surf. Coat. Technol. **120–121**, 401–404 (1999).
[3] A. V. Arefiev and B. N. Breizman, "Theoretical components of the VASIMR plasma propulsion concept," Phys. Plasmas **11**, 2942–2949 (2004).
[4] J. P. Squire, "Investigation of a light gas helicon plasma source for the VASIMR space propulsion system," AIP Conf. Proc. **694**, 423–426 (2003).
[5] J. F. Caneses and B. D. Blackwell, "Collisional damping of helicon waves in a high density hydrogen linear plasma device," Plasma Sources Sci. Technol. **25**, 055027 (2016).
[6] J. B. O. Caughman, R. H. Goulding, T. M. Biewer, T. S. Bigelow, I. H. Campbell, J. Caneses, S. J. Diem, A. Fadnek, D. T. Fehling, R. C. Isler, E. H. Martin, C. M. Parish, J. Rapp, K. Wang, C. J. Beers, D. Donovan, N. Kafle, H. B. Ray, G. C. Shaw, and M. A. Showers, "Plasma source development for fusion-relevant material testing," J. Vac. Sci. Technol. A **35**, 03E114 (2017).
[7] A. Simonin, J. Achard, K. Achkasov, S. Bechu, C. Baudouin, O. Baulaigue, C. Blondel, J. P. Boeuf, D. Bresteau, G. Cartry, A. Jocelyn, K. Achkasov, S. Bechu, C. Baudouin, O. Baulaigue, C. Blondel, J. P. Boeuf, D. Bresteau, G. Cartry, W. Chaibi, C. Drag, H. P. L. de Esch, D. Fiorucci, G. Fubiani, I. Furno, R. Futtersack, P. Garibaldi, A. Gicquel, C. Grand, G. Ph, G. Hagelaar, A. Howling, R. Jacquier, M. J. Kirkpatrick, D. Lemoine, B. Lepetit, T. Minea, E. Odic, A. Revel, B. A. Soliman, and P. Teste, "R&D around a photoneutralizer-based NBI system (Siphore) in view of a DEMO Tokamak steady state fusion reactor," Nucl. Fusion **55**, 123020 (2015).
[8] J. Santoso, R. Manoharan, S. O'Byrne, and C. S. Corr, "Negative hydrogen ion production in a helicon plasma source," Phys. Plasmas **22**, 093513 (2015).
[9] K. P. Shamrai and V. B. Taranov, "Volume and surface rf power absorption in a helicon plasma source," Plasma Sources Sci. Technol. **5**, 474–491 (1996).
[10] P. K. Loewenhardt, B. D. Blackwell, R. W. Boswell, G. D. Conway, and S. M. Hamberger, "Plasma production in a toroidal heliac by helicon waves," Phys. Rev. Lett. **67**, 2792–2794 (1991).
[11] A. W. Molvik, A. R. Ellingboe, and T. D. Rognlien, "Hot-electron production and wave structure in a helicon plasma source," Phys. Rev. Lett. **79**, 233–236 (1997).
[12] D. D. Blackwell, T. G. Madziwa, D. Arnush, and F. F. Chen, "Evidence for Trivelpiece-Gould modes in a helicon discharge," Phys. Rev. Lett. **88**, 145002 (2002).
[13] B. Breizman and A. Arefiev, "Radially localized helicon modes in nonuniform plasma," Phys. Rev. Lett. **84**, 3863–3866 (2000).
[14] F. F. Chen and D. D. Blackwell, "Upper limit to Landau damping in helicon discharges," Phys. Rev. Lett. **82**, 2677–2680 (1999).
[15] J. L. Kline, E. E. Scime, R. F. Boivin, A. M. Keesee, X. Sun, and V. S. Mikhailenko, "rf absorption and ion heating in helicon sources," Phys. Rev. Lett. **88**, 195002 (2002).
[16] D. Arnush, "The role of TrivelpieceGould waves in antenna coupling to helicon waves," Phys. Plasmas **7**, 3042 (2000).
[17] F. F. Chen and D. Curreli, "Central peaking of magnetized gas discharges," Phys. Plasmas **20**, 057102 (2013).
[18] K. P. Shamrai, "Stable modes and abrupt density jumps in a helicon plasma source," Plasma Sources Sci. Technol. **7**, 499–511 (1998).
[19] D. Curreli and F. F. Chen, "Equilibrium theory of cylindrical discharges with special application to helicons," Phys. Plasmas **18**, 113501 (2011).
[20] Y. Sakawa, T. Takino, and T. Shoji, "Contribution of slow waves on production of high-density plasmas by m=0 helicon waves," Phys. Plasmas **6**, 4759 (1999).
[21] R. H. Goulding, J. B. O. Caughman, J. Rapp, T. M. Biewer, T. S. Bigelow, I. H. Campbell, J. F. Caneses, D. Donovan, N. Kafle, E. H. Martin, H. B. Ray, G. C. Shaw, and M. A. Showers, "Progress in the development of a high power helicon plasma source for the materials plasma exposure experiment," Fusion Sci. Technol. **72**, 588–594 (2017).
[22] J. F. Caneses and B. Blackwell, "RF compensation of double Langmuir probes: Modelling and experiment," Plasma Sources Sci. Technol. **24**, 035024 (2015).
[23] R. Ochoukov, V. Bobkov, H. Faugel, H. Fünfgelder, and J. Noterdaeme, "A new B-dot probe-based diagnostic for amplitude, polarization, and wavenumber measurements of ion cyclotron range-of frequency fields on ASDEX Upgrade," Rev. Sci. Instrum. **86**, 115112 (2015).
[24] C. M. Franck, O. Grulke, and T. Klinger, "Magnetic fluctuation probe design and capacitive pickup rejection," Rev. Sci. Instrum. **73**, 3768 (2002).
[25] M. Showers, T. M. Biewer, J. B. O. Caughman, D. C. Donovan, R. H. Goulding, and J. Rapp, "Heat flux estimates of power balance on Proto-MPEX with IR imaging," Rev. Sci. Instrum. **87**, 11D412 (2016).
[26] S. I. Braginskii, "Transport processes in a plasma," Rev. Plasma Phys. **1**, 205 (1965), http://people.hao.ucar.edu/judge/homepage/PHSX515/fall2012/Braginskii1965.pdf.
[27] M. D. Carter, F. W. Baity, G. C. Barber, R. H. Goulding, Y. Mori, D. O. Sparks, K. F. White, E. F. Jaeger, F. R. Chang-Díaz, and J. P. Squire, "Comparing experiments with modeling for light ion helicon plasma sources," Phys. Plasmas **9**, 5097–5110 (2002).
[28] K. Niemi and M. Krämer, "Helicon mode formation and radio frequency power deposition in a helicon-produced plasma," Phys. Plasmas **15**, 073503 (2008).
[29] J. F. Caneses, B. D. Blackwell, and P. Piotrowicz, "Helicon antenna radiation patterns in a high density hydrogen linear plasma device," Phys. Plasmas **24**, 113513 (2017).
[30] A. I. Akhiezer, V. S. Mikhailenko, and K. N. Stepanov, "Ion-sound parametric turbulence and anomalous electron heating with application to helicon plasma sources," Phys. Lett. A **245**, 117–122 (1998).
[31] F. F. Chen, "Physics of helicon discharges," Phys. Plasmas **3**, 1783–1793 (1996).